ADVANCED MATERIALS

Supporting Information

for *Adv. Mater.*, DOI: 10.1002/adma.201701432

Simultaneous Enhancement of Charge Separation and Hole Transportation in a TiO_2–$SrTiO_3$ Core–Shell Nanowire Photoelectrochemical System

Fei Wu, Yanhao Yu, Huang Yang, Lazarus N. German, Zhenquan Li, Jianguo Chen, Weiguang Yang, Lu Huang, Weimin Shi, Linjun Wang,* and Xudong Wang**

Supporting Information

Simultaneous Enhancement of Charge Separation and Hole Transportation in TiO_2-$SrTiO_3$ Core-Shell Nanowire Photoelectrochemical System

Fei Wu, Yanhao Yu, Huang Yang, Lazarus N. German, Zhenquan Li, Jianguo Chen, Weiguang Yang, Lu Huang, Weimin Shi, Linjun Wang,*and Xudong Wang**

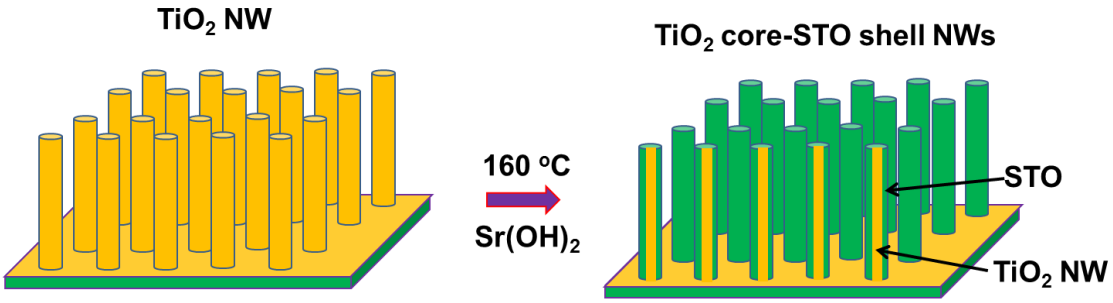

Figure S1. Schematic fabrication process of TiO_2/STO core-shell NWs

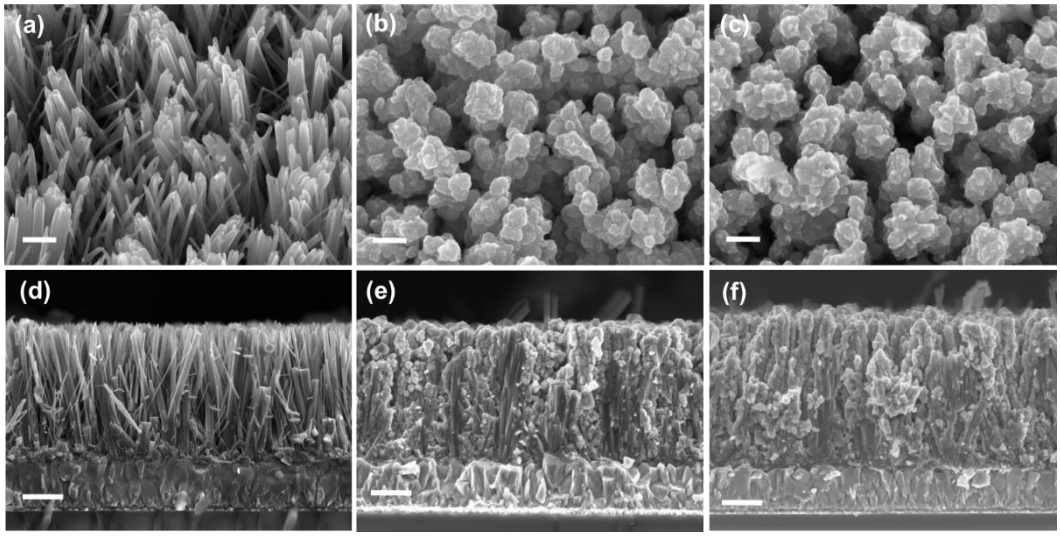

Figure S2. (a-c) 15°-tilted view and **(d-f)** cross-sectional SEM images of TiO_2/STO NWs obtained after 1-hour (a,d), 3-hour (b,e) and 4-hour (c,f) hydrothermal conversion at 160 ℃. Scale bars: 200 nm (tilted-view) and 500 nm (cross-sectional).

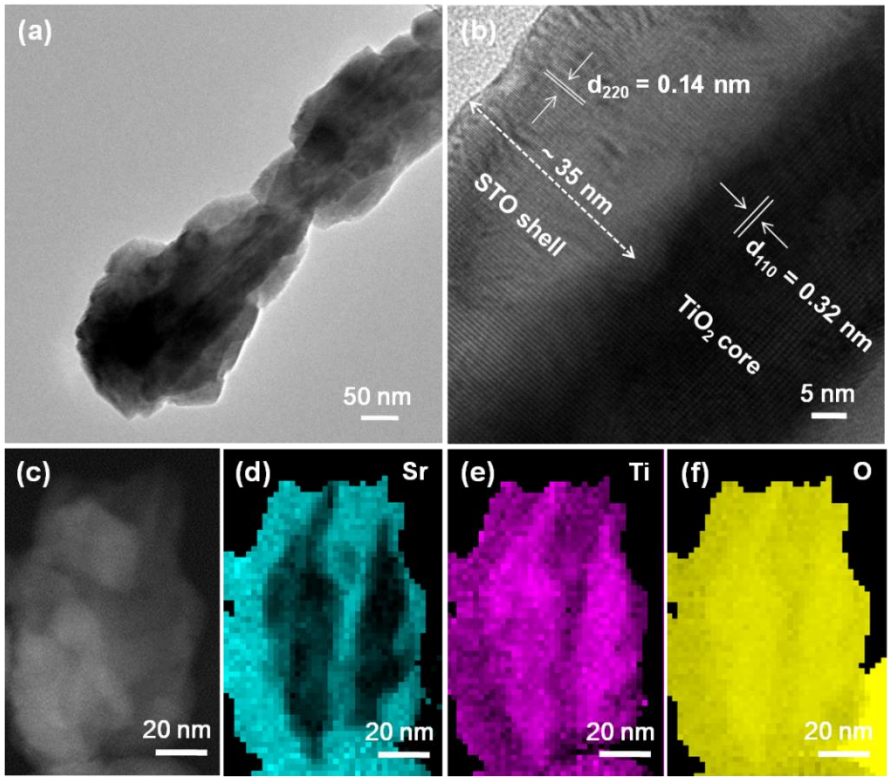

Figure S3. Structural and elemental characterizations of the TiO_2 core-STO shell NW prepared at 160 ^oC for 4h (35 nm STO shell thickness). **(a)** Representative TEM image of a TiO_2/35 nm STO NW. **(b)** HRTEM images of the TiO_2/35 nm STO NW along the edge, showing a single-crystalline STO shell with a thickness ~35 nm. The clear lattice fringes with spacing of 0.14 and 0.32 nm are indexed to the (220) plane of STO and (110) plane of the rutile TiO_2, respectively. **(c)** STEM image of the tip region of a TiO_2/35 nm STO NW. **(d-f)** Corresponding EELS elemental mapping of Sr **(d)**, Ti **(e)** and O **(f)**, respectively.

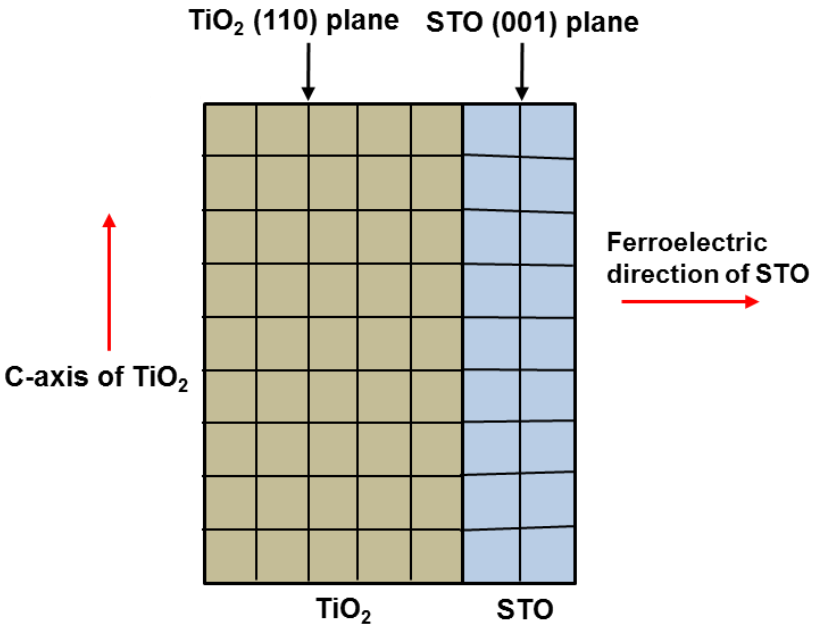

Figure S4. Schematic illustration of the relationship between c-axis of TiO_2 and the ferroelectric polarization direction of STO.

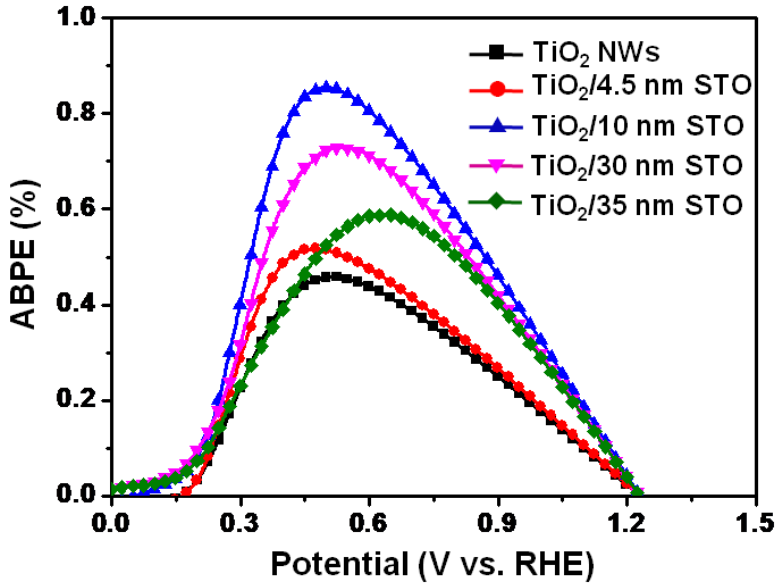

Figure S5. Applied bias photon-to-current efficiency (ABPE) as a function of applied potential obtained using a three-electrode system.

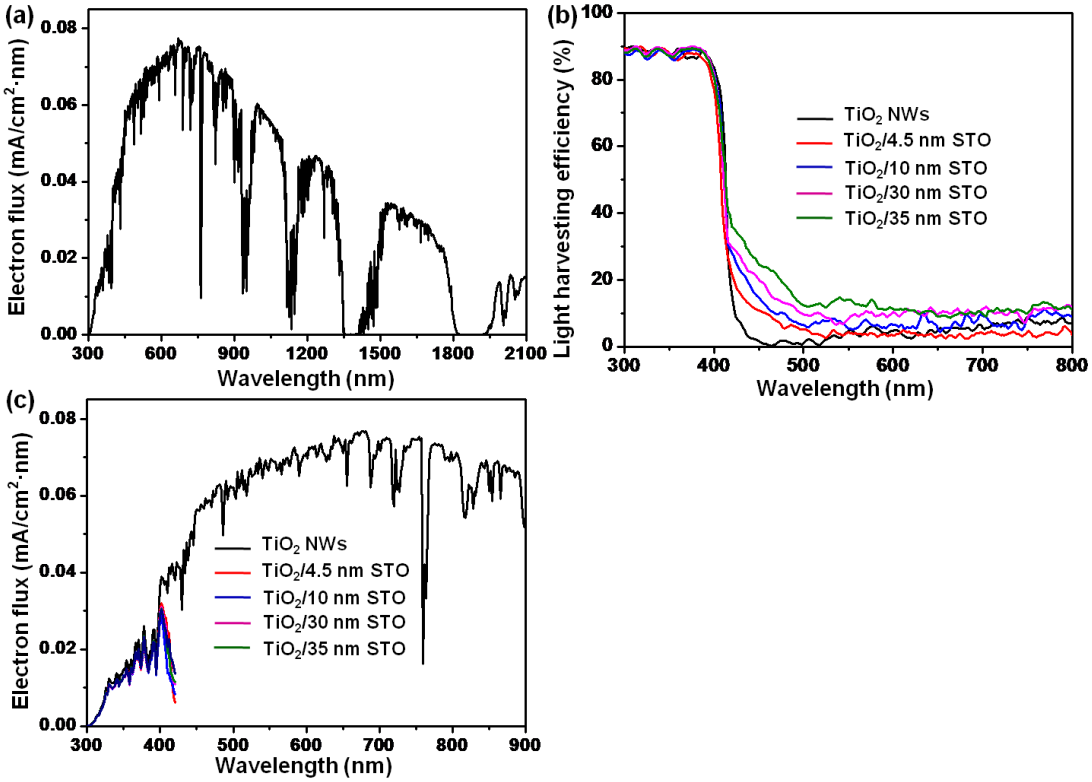

Figure S6. (a) Electron flux of AM 1.5G solar spectrum. **(b)** The light harvesting efficiencies (η_{LHE}) calculated from the absorption data (η_{ABS}) shown in **(a)** via the equation $\eta_{LHE} = (1\text{-}10^{-\eta ABS}) \times 100\%$. **(c)** Electron flux of the pristine TiO_2 NW and TiO_2/4.5, 10, 30 and 35 nm STO core-shell NW photoanodes.

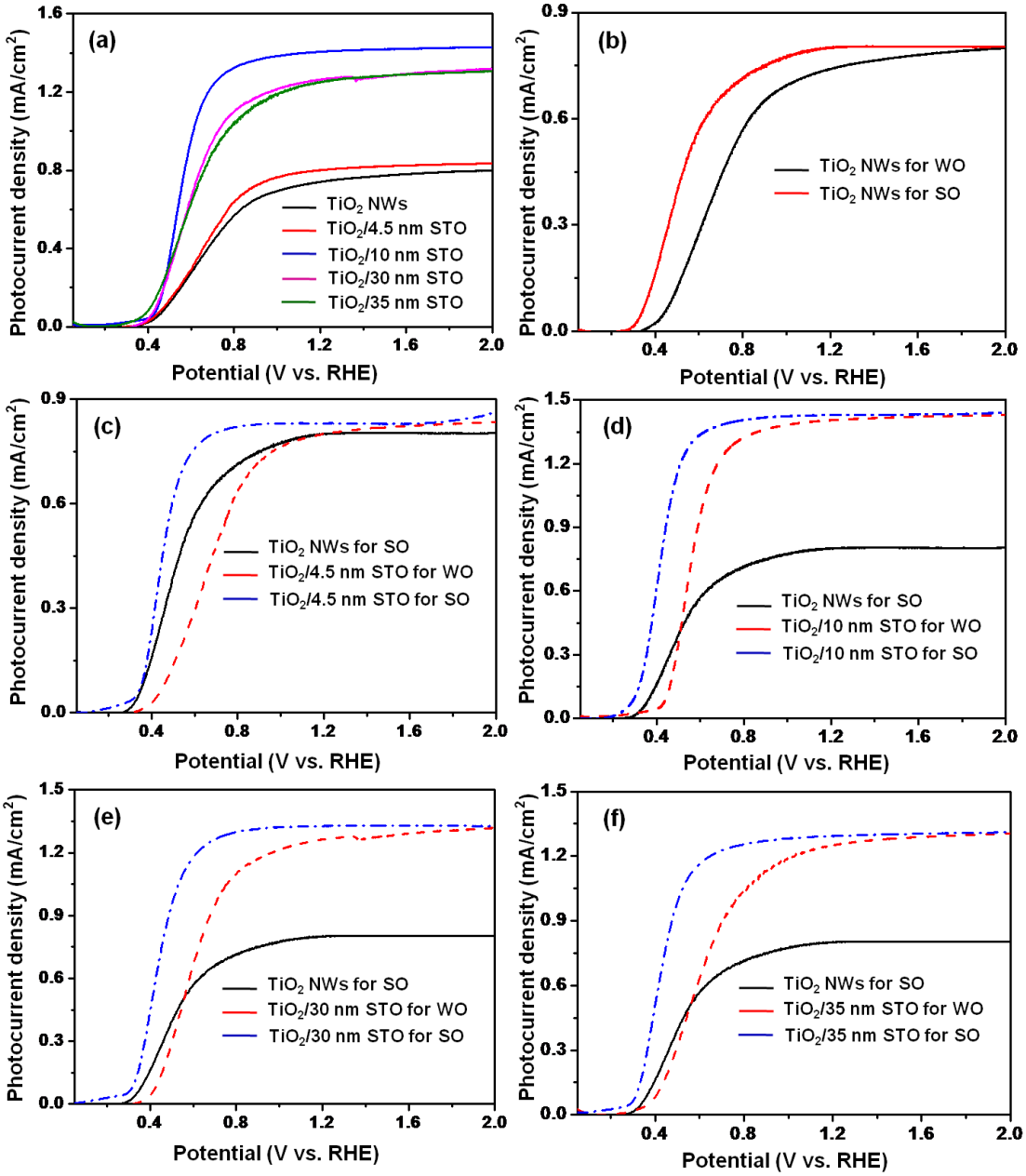

Figure S7. (a) *J-V* curves of the prinstine TiO_2 NW array and TiO_2/STO core-shell NW arrays with four different STO thickness for water oxidation (WO) measured in a 0.5 M phosphate buffer (pH = 7) under AM 1.5 G illumination (100 mW/cm^2). **(b-f)** Comparison of *J-V* curves measured for WO and in a 0.5 M phosphate buffer (pH = 7) and sulfite oxidation (SO) measured in a 0.5 M phosphate buffer with 1 M Na_2SO_3 (pH = 7) as the hole scavenger under AM 1.5 G illumination. Comparisons were made between the pristine TiO_2 NW arrays **(b)** and TiO_2-STO core/shell NW arrays with STO thickness of 4.5 **(c)**, 10 **(d)**, 30 **(e)** and 35 **(f)** nm.

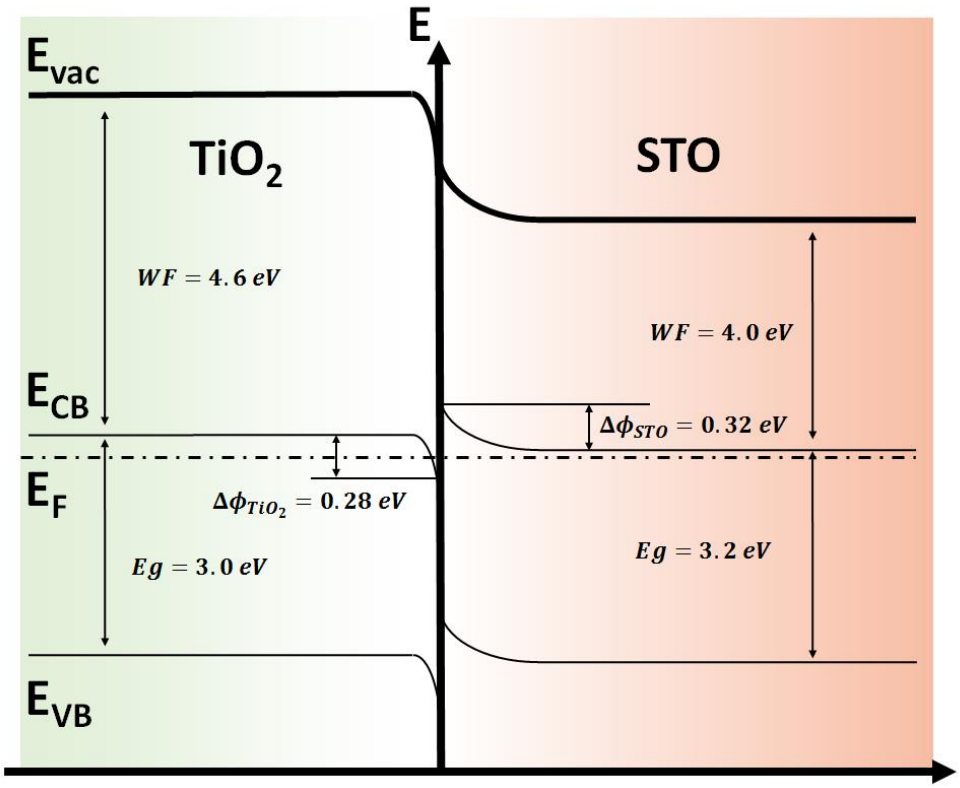

Figure S8. Schematic band structure at the TiO_2/STO interface.

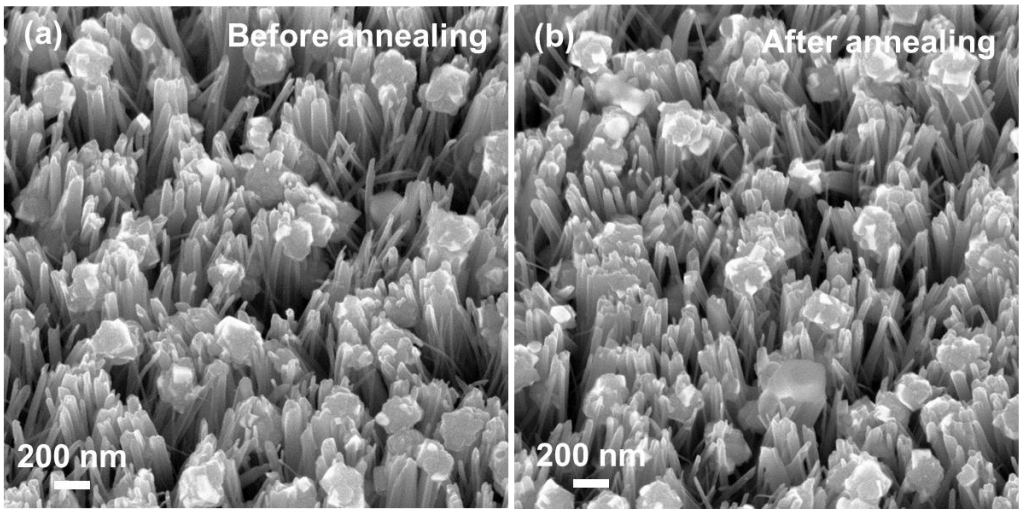

Figure S9. SEM images of TiO_2/10 nm STO NWs before **(a)** and after **(b)** annealing at 500 °C for 1 hours.

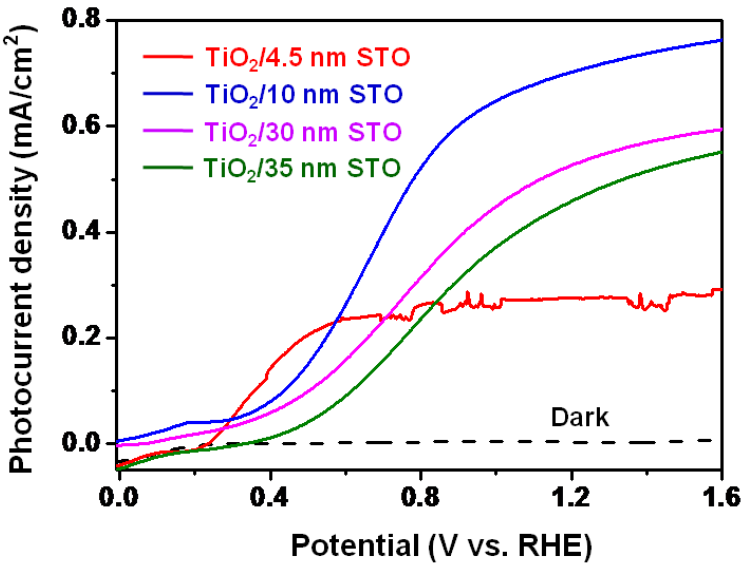

Figure S10. *J-V* curves of the TiO_2/4.5, 10, 30 and 35 nm STO annealed at 500 ºC for 1h.

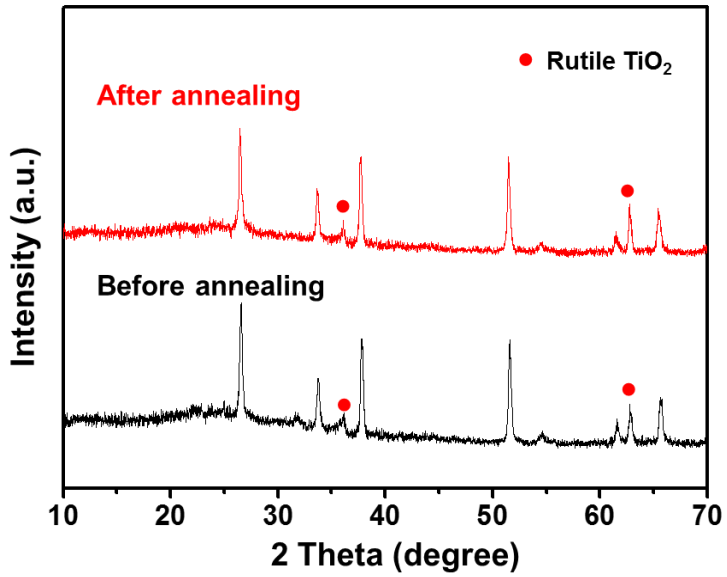

Figure S11. XRD of TiO_2 NWs before (black) and after (red) annealing at 500 °C for 1 hours.

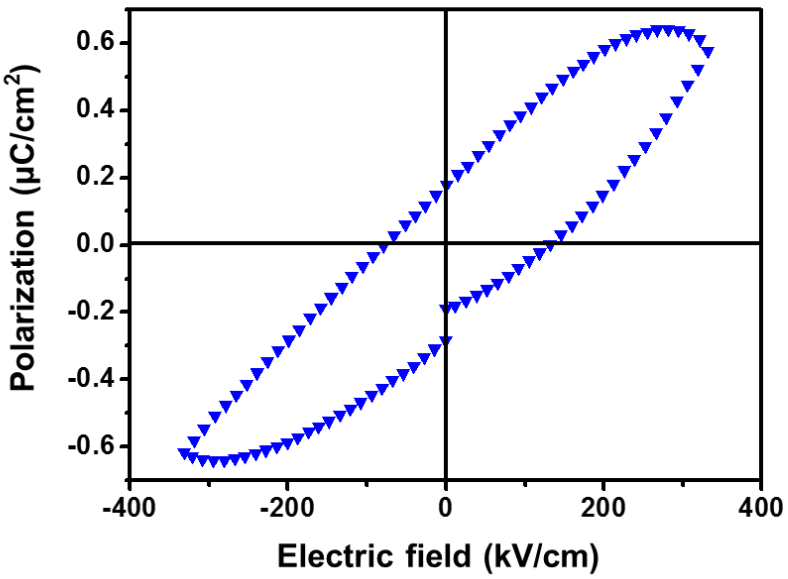

Figure S12. Polarization-electric field loop of the TiO_2/35 nm STO NWs.

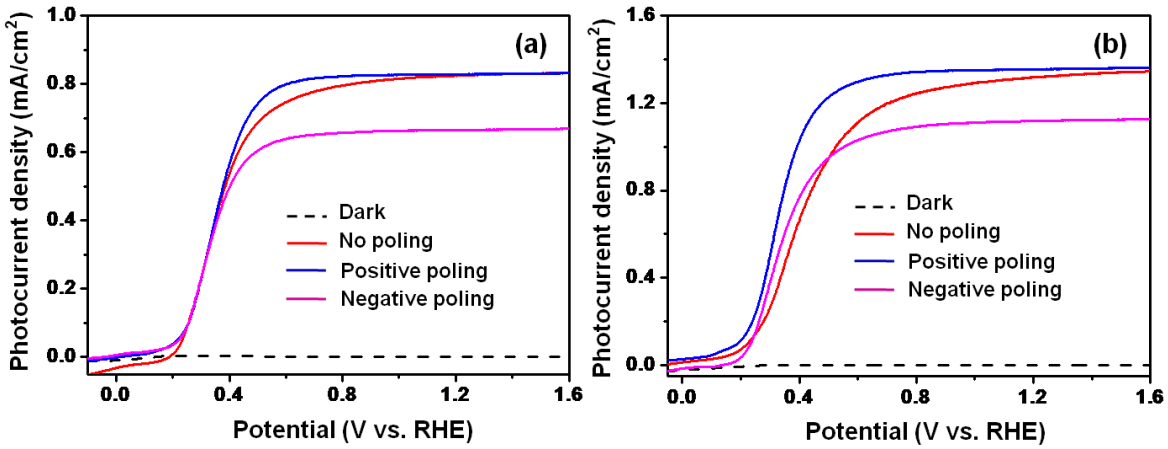

Figure S13. *J-V* curves of the as-prepared (red), positively poled (blue) and negatively poled (magenta) TiO_2 core-STO shell NW arrays prepared at 160 °C with the STO thickness of 4.5 nm **(a)** and 30 nm **(b)** measured in a 1 M NaOH solution (pH = 13.6) under AM 1.5 G illumination (100 mW/cm^2) using three electrode setup. The as-prepared samples were poled under ± 10 V in air.